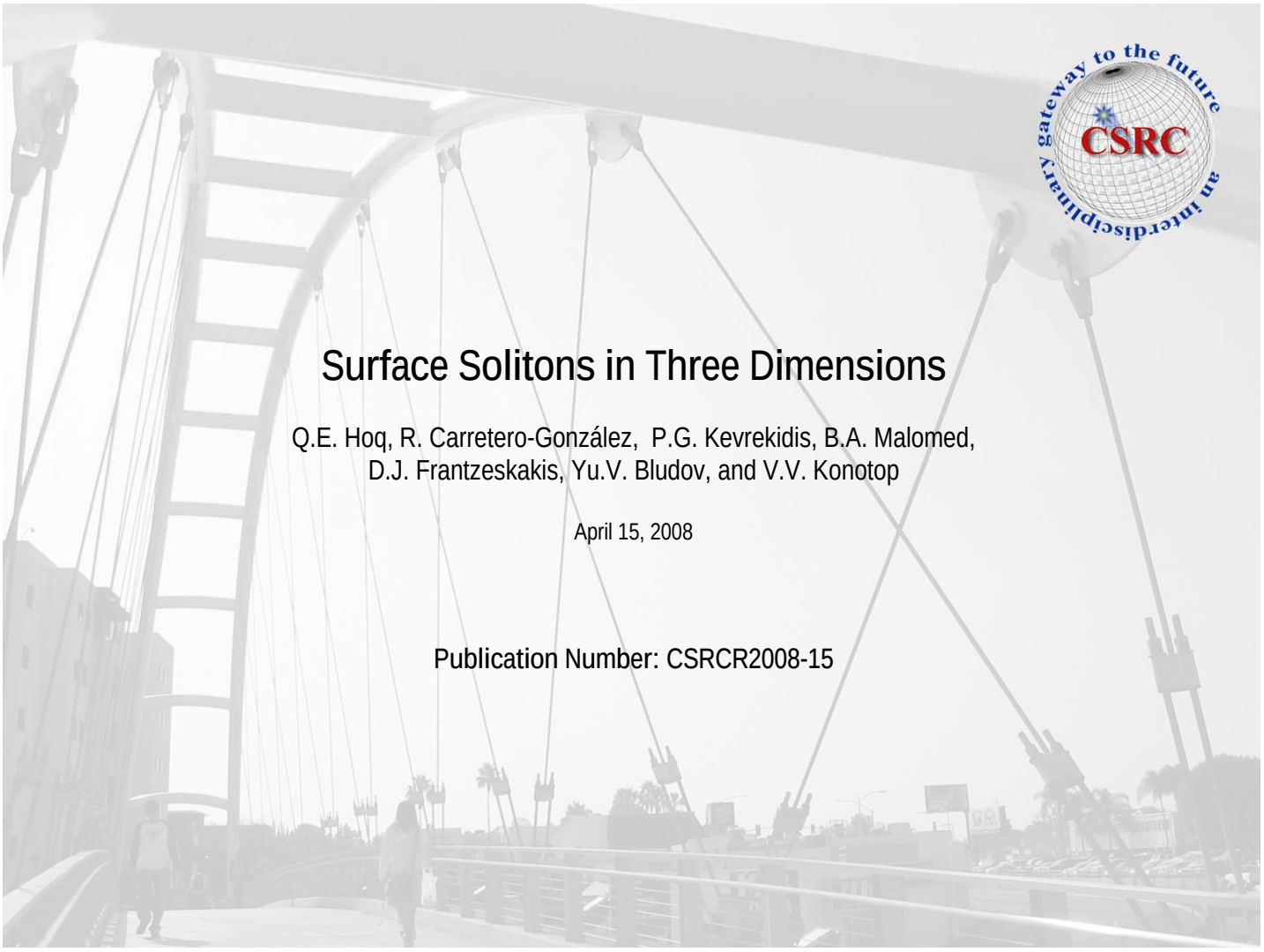

Surface Solitons in Three Dimensions

Q.E. Hoq, R. Carretero-González, P.G. Kevrekidis, B.A. Malomed,
D.J. Frantzeskakis, Yu.V. Bludov, and V.V. Konotop

April 15, 2008

Publication Number: CSRCR2008-15

Computational Science & Engineering Faculty and Students Research Articles

Database Powered by the Computational Science Research Center Computing Group & Visualization Lab

COMPUTATIONAL SCIENCE & ENGINEERING

SAN DIEGO STATE UNIVERSITY

Computational Science Research Center
College of Sciences
5500 Campanile Drive
San Diego, CA 92182-1245
(619) 594-3430

Surface Solitons in 3 Dimensions

Q.E. Hoq,[1] R. Carretero-González,[2] P.G. Kevrekidis,[3] B. A. Malomed,[4] D. J. Frantzeskakis,[5] Yu. V. Bludov,[6] and V. V. Konotop[6]

[1]*Department of Mathematics, Western New England College, Springfield, MA, 01119, USA*
[2]*Nonlinear Dynamical Systems Group**, *Department of Mathematics and Statistics, and Computational Science Research Center, San Diego State University, San Diego CA, 92182-7720, USA*
[3]*Department of Mathematics and Statistics, University of Massachusetts, Amherst MA 01003-4515, USA*
[4]*Department of Physical Electronics, Faculty of Engineering, Tel Aviv University, Tel Aviv 69978, Israel*
[5]*Department of Physics, University of Athens, Panepistimiopolis, Zografos, Athens 157 84, Greece*
[6]*Centro de Física Teórica e Computacional, Universidade de Lisboa, Complexo Interdisciplinar, Avenida Professor Gama Pinto 2, Lisboa 1649-003, Portugal*

In this paper we study localized modes on the surface of a three dimensional lattice. We numerically compare the stability of these structures with the corresponding bulk solitons. Typically, the surface increases the region of stability. An extreme example of this being the 3 site horseshoe, which is completely unstable in the bulk, while at the surface it is stable near the anti-continuum limit. We also examine the effect of the surface on a lattice vortex. It is noted that when parallel to the surface the same stabilizing effect as above is observed, while it cannot exist normal to the surface.

I. INTRODUCTION

Surface waves have been observed and studied in a variety of areas such as physics (surface plasmons on a conductor [1], and optical solitons in waveguide arrays [2]), chemistry (surface waves in magnetic isotropic magnetic gels) [3] and biology (ocean water waves). Often times the properties and features exhibited by such modes have no analogue in the corresponding bulk media, and thus makes their study both interesting and relevant. Of particular interest here are nonlinear surface waves in optics, which have been extensively studied. It has been theoretically shown [4] and experimentally observed [5] that discrete nonlinear waves can be supported at the edge of a semi-infinite array of nonlinear optical waveguide arrays. Such solitary waves were predicted to exist not only in focusing media as in the references discussed above, but also between uniform and self-defocusing media in [4, 6] and were subsequently observed both for quadratic [7] and for photorefractive [8, 9] nonlinearities. In the 2D setting, stable topological solitons have been predicted in a saturable medium [10], which constitute generalizations to stable asymmetric vortex solitons predicted in Ref. [11]. Stable discrete vortex solitons have been experimentally observed in a self-focusing bulk photorefractive media in [12]. Results for a variety of species of discrete surface solitons in 2D was reported in Ref. [13–16]. It was observed there that the surface can have a stabilizing effect on ordinary solitons, while impeding the existence of some. Subsequent work resulted in the experimental observation of 2D surface solitons (both of the fundamental and of multi-pulse soliton structures) in photorefractive media [17], as well as in asymmetric waveguide arrays in fused silica [18]. More recently, surface solitons in more complex settings such as chirped optical lattices in 1d and 2d [19, 20], between photonic crystals and metamaterials [21] and even in nonlocal settings [22, 23] have emerged.

To the best of our knowledge, however, most of these efforts have been constrained to 1d or 2d settings. The only 3d setting examined was that of truncated 2d photonic lattices incorporating the effect of time evolution to produce 3d "surface light bullets" in [24] (the corresponding 2d surface structures were examined in [25]). Our aim in the present paper is to extend the latter setting to surface solitons in genuinely 3d lattices which may be relevant e.g., to crystals built of microresonators trapping photons [26] or polaritons [27], or to Bose-Einstein condensates in the vicinity of 2d surface of a 3d optical lattice [28, 29]. In particular, in this manuscript we report results for surface solitons at the surface of a 3D lattice: we study 3D solitons that are analogous of those studied in Ref. [13] such as dipoles and 3 site horseshoes, and also look at some configurations that are specific to a 3D lattice. A variety of species of solitons will be examined and their stability on the surface will be compared to that in the bulk. In some cases, e.g. the dipole, the soliton may be placed either normal or parallel to the surface. Typically, increased contact with the surface increases the region of stability of the structure. This is qualitatively reasonable, since the surface allows interactions with fewer neighbors, rendering the system "more discrete", and hence in our case more stable. In some cases, this effect becomes more pronounced as e.g. in the 3-site horseshoes which are never stable in the bulk but become stabilized in the presence of the surface. In some other cases, the surface may have an adverse effect, inhibiting the existence of a particular mode. As such an example, we note the discrete vortex (see below), which when parallel to the surface has increased stability as compared to the bulk mode, but when normal to the surface, it cannot exist.

The model we examine here is based on the discrete

*URL: http://nlds.sdsu.edu

nonlinear Schrödinger (DNLS) equation on the 3D lattice:

$$i\dot{\phi}_{m,n,l} + \varepsilon\Delta^{(3)}\phi_{m,n,l} + |\phi_{m,n,l}|^2\phi_{m,n,l} = 0 \quad (1)$$

where $\phi_{m,n,l}$ is the complex field, ε is the coupling constant, $\dot{\phi} = d\phi/dz$, and $\Delta^{(3)}\phi_{m,n,l}$ is the discrete Laplacian in 3D:

$$\Delta^{(3)}\phi_{m,n,l} \equiv \phi_{m+1,n,l} + \phi_{m-1,n,l} + \phi_{m,n+1,l} + \phi_{m,n-1,l} + \phi_{m,n,l+1} + \phi_{m,n,l-1} - 6\phi_{m,n,l}. \quad (2)$$

for $l \geq 2$ and all m, n. Along the surface, $l = 1$, the discrete Laplacian is modified by dropping the term with subscript index $l-1$.

We look for stationary solutions $\phi_{m,n,l} = \exp(i\Lambda z)u_{m,n,l}$. The steady state equation corresponding to Eq. (1) is then

$$(\Lambda - |u_{m,n,l}|^2)u_{m,n,l} - \varepsilon\Delta^{(3)}u_{m,n,l} = 0. \quad (3)$$

Our presentation will be structured as follows. In the following section, we will briefly summarize the theoretical background for the theoretical existence and stability predictions that will follow. We then provide a bifurcation analysis of the various structures of interest at the surface (in comparison with their bulk siblings) as a function of the coupling parameter ε in section III. Section IV illustrates the instability dynamics of the surface structures. Finally, section V summarizes our findings and presents our conclusions.

II. THEORETICAL BACKGROUND

We find solution families by starting from the anti-continuum (AC) limit, $\varepsilon = 0$ [30]. In the anti-continuum limit, we consider only a few excited sites which determine the profile of the configuration. The continuation of the structure to $\varepsilon > 0$ is determined from the Lyapunov Reduction Theorem [31]. More specifically, the solution is expanded as a power series in ε and the solvability condition at each order is that the projection to the kernel of the previous order in the reduction will yield no secular terms [30].

Linear stability is then determined using the perturbation ansatz

$$\phi_{m,n,l} = e^{i\Lambda z}(u_{m,n,l} + \delta a_{m,n,l}e^{-i\omega z} + \delta b_{m,n,l}e^{i\omega^* z}), \quad (4)$$

where δ is a formal small parameter, ω is the corresponding eigenvalue with associated eigenvector $\{a_{m,n,l}, b^*_{m,n,l}\}$ and $(\cdot)^*$ stands for complex conjugation. Substituting this ansatz into Eq. (1) yields the following linearized system:

$$\begin{aligned} -\omega a_{m,n,l} &= -\varepsilon\Delta^{(3)}a_{m,n,l} + \Lambda a_{m,n,l} - 2|u_{m,n,l}|^2 a_{m,n,l} \\ &\quad - u^2_{m,n,l}b^*_{m,n,l} \\ \omega^* b_{m,n,l} &= -\varepsilon\Delta^{(3)}b_{m,n,l} + \Lambda b_{m,n,l} - 2|u_{m,n,l}|^2 b_{m,n,l} \\ &\quad - u^2_{m,n,l}a^*_{m,n,l} \end{aligned} \quad (5)$$

This system can be written as

$$\sigma\mathcal{H}\psi = i\lambda\psi, \quad (6)$$

where $\lambda = i\omega$. Here σ is the matrix consisting of the 2×2 blocks

$$\sigma_{n,m} = \begin{pmatrix} 0 & 1 \\ -1 & 0 \end{pmatrix}\delta_{n,m}, \quad (7)$$

and the matrix $\mathcal{H}$ has entries:

$$\begin{aligned} \mathcal{H}_{n,m} &= \begin{pmatrix} 1-2|v_{n,m}|^2 & -v^2_{n,m} \\ -\bar{v}^2_{n,m} & 1-2|v_{n,m}|^2 \end{pmatrix} \\ &\quad - \epsilon\left(s_{+1,0} + s_{-1,0} + s_{0,+1} + s_{0,-1}\right)\begin{pmatrix} 1 & 0 \\ 0 & 1 \end{pmatrix}. \end{aligned} \quad (8)$$

It is shown in Ref. [30], that the linear stability eigenvalues of the full problem, λ, are related to the eigenvalues, γ, of the matrix $\mathcal{H}$, to leading order through the equation $\lambda = \sqrt{2\gamma}\epsilon^{s/2}$, where s is the number of lattice sites that separate adjacent excited nodes of the configuration at the AC limit.

III. BIFURCATION ANALYSIS

In this section we numerically exhibit the existence and stability of various 3D configurations and compare these results with the corresponding analytical predictions. These configurations are obtained by starting from the AC limit ($\varepsilon = 0$), and are continued for small $\varepsilon > 0$, by using a fixed point iteration. For all the numerical results presented in this work we choose without loss of generality $\Lambda = 1$ and we use a lattice of $13 \times 13 \times 13$ unless stated otherwise. We start by examining parallel and normal surface dipoles. In Fig. 1, the top panel shows the norm ($N = \sum_{l,n,m}|u_{m,n,l}|^2$) versus the coupling ε while the second panel depicts the imaginary part of the linear stability eigenvalue for the bulk dipole from the theory described in the previous section (black dashed line) and from the numerics (solid blue line). The theoretical prediction for the stability eigenvalues is $\lambda = \pm2\sqrt{\varepsilon}i$, which, as expected is the same as in an out of phase (so-called twisted) 1D mode analyzed in [32], as the structure is essentially 1D along the line connecting the two excited sites. The third panel in the figure compares the largest instability growth rate (versus ε) for the bulk (dash-dotted line), normal (dashed line) and parallel dipoles (solid line). It is seen that the interval of stability of the dipole is increased with increased contact with the surface, as rationalized above. In the case of a bulk dipole, the instability sets in between $\varepsilon_0 = 0.114$ and $\varepsilon_1 = 0.115$. From now on, when reporting the computed instability thresholds, we will use the lower bound for ε (cf., ε_0 in the previous example) and the accuracy of our numerical computation (i.e., the chosen ε-step) will be denoted by a number in parenthesis after the reported threshold. Thus, using this notation, the threshold for the bulk

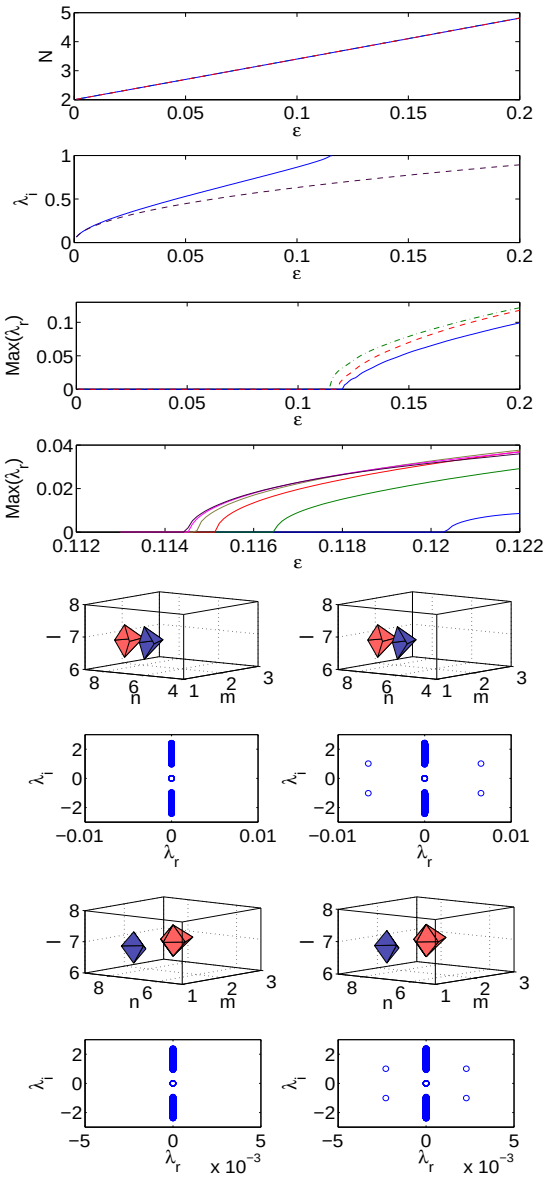

FIG. 1: (Color Online) Features for the parallel and normal surface dipoles. The top panel shows the norm N versus the coupling ε. The second panel shows the imaginary part of the linear stability eigenvalue and compares the numerical (solid blue line) and analytical results (black dashed line). The third panel depicts the real part of the critical (in)stability eigenvalue. The red dashed and blue solid lines depict the normal and parallel surface dipoles respectively, while the green dash-dotted line corresponds to the bulk dipole. The fourth panel depicts the (in)stability eigenvalue for the parallel surface dipole when placed at distances starting at the surface up to 5 units away (curves right to left). The bottom two sets of four panels show the configurations (respective top panels) and spectral stability plane (respective bottom panels) just before (respective left panels) and just after (respective right panels) the stability threshold. The level contours shown corresponding to $\mathrm{Re}(u_{l,m,n}) = \pm 0.5 \max\{u_{m,n,l}\}$ are shown, respectively, in blue and red (dark gray and gray, in the black-and-white version). The thresholds for the parallel and normal dipoles are, respectively, $\varepsilon = 0.117(1)$ and $\varepsilon = 0.120(1)$. For comparison, the threshold for the bulk dipole is $\varepsilon = 0.114(1)$.

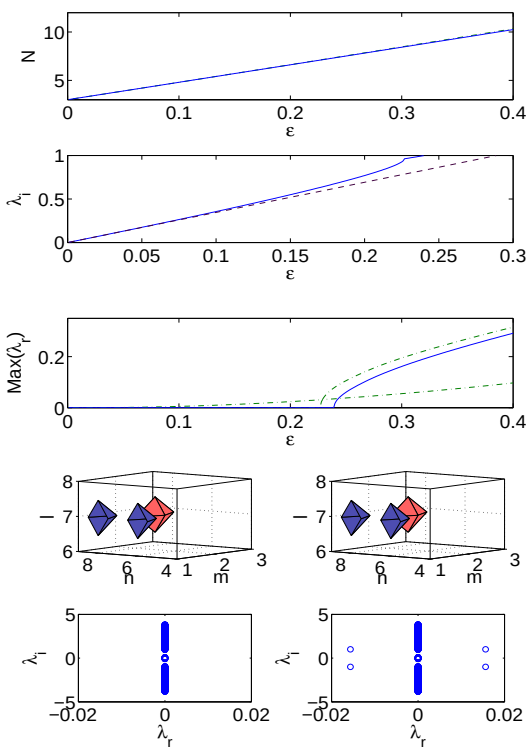

FIG. 2: Stability for the 3 site horseshoe. The panels are similar to those in Fig. 1. The third panel compares the critical stability eigenvalue versus the lattice coupling for the surface horseshoe (solid line) with the bulk (dash-dotted line). It is seen that the bulk horseshoe is always unstable (due to a higher order eigenvalue), while the corresponding surface configuration has a region of stability (the corresponding eigenvalue becomes imaginary in this case). The bottom set of four panels corresponds to the surface horseshoe just before (left) and just after (right) the stability threshold at $\varepsilon = 0.239(1)$.

dipole is $\varepsilon = 0.114(1)$. For the normal dipole, we observe the instability at $\varepsilon = 0.117(1)$, while for the parallel one at $\varepsilon = 0.120(1)$. In Fig. 1, we also depict (see the bottom two sets of four panels) the normal and parallel surface dipole, just before and just after the instability threshold along with the corresponding spectral stability planes.

The surface (stabilizing) effects depend in great measure on the distance of the configuration to the surface. The further away the configuration is from the surface the lesser the effect. This natural phenomenon is clearly seen in the fourth panel of Fig. 1 where we plot the (in)stability eigenvalue as a function of the coupling for *several* distances of a parallel surface dipole. The curves, from right to left, depict results for a dipole 0, 1, ..., 5 sites away from the surface (0 sites away from the surface refers to a surface dipole). As the panel indicates, the stability interval is reduced as the dipole is pulled away from the surface converging towards a bulk dipole.

Let us now turn our attention to a type of configuration for which the surface may play a critical role on their stability, namely horseshoes. In Fig. 2 we depicted the

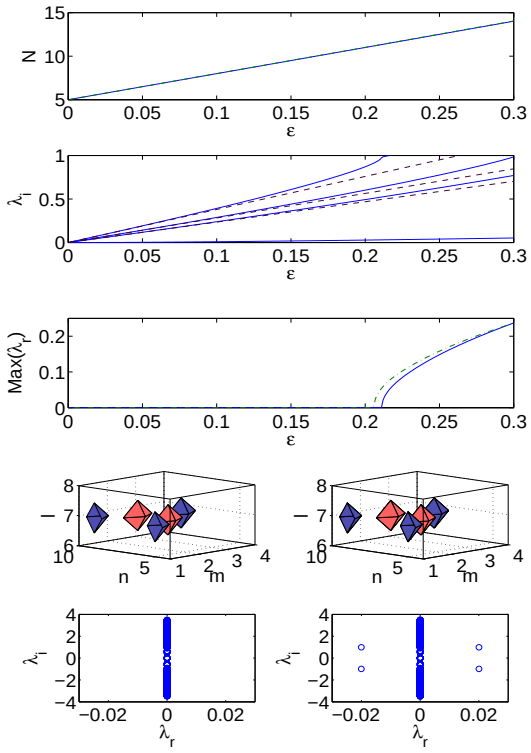

FIG. 3: Stability for the 5 site horseshoe. The panels are identical to those in Fig. 2. In this case the stability threshold occurs at $\varepsilon = 0.211(1)$. For reference, the bulk 5 site horseshoe destabilizes at $\varepsilon = 0.205(1)$. The bottom four panels depict the configuration an its stability spectrum just before (left, $\varepsilon = 0.211$) and just after (right, $\varepsilon = 0.212$) the destabilization.

properties of a 3 site horseshoe that is a truncated version of a quadrupole. As before, the first panel in Fig. 2 shows the norm versus ε, while the second and third panels compare the stability results for the bulk horseshoe (dash-dotted line) to the surface one (solid line). Numerically we see that the bulk structure is always unstable, similarly to its 2D analog [13]. However, its surface counterpart is stable for small ε, eventually destabilizing at $\varepsilon = 0.239(1)$. The lower set of four panels in Fig. 2 shows the configurations for the coupling just before and just after the point of instability, along with the corresponding spectral planes. The stable eigenvalues are found to be $\lambda = 0$, $\lambda = \pm 2\sqrt{3}\varepsilon i$, $\lambda = \mathcal{O}(\varepsilon^2)$ (cf. [13]).

Fig. 3 illustrates the same features as before but for the 5 site horseshoe. Unlike its three site cousin, the bulk 5 site horseshoe is stable for up to a critical value of the coupling, with the surface variant showing increased stability. In the bulk the 5 site horseshoe becomes unstable at $\varepsilon = 0.205(1)$, while on the surface, the corresponding threshold is $\varepsilon = 0.211(1)$. The stability eigenvalues in this case can be computed analogously to the 3-site case [13], as outlined in the theoretical section above (cf. also [30]) and are $\lambda = 3.8042\varepsilon i$, $\lambda = 2.8284\varepsilon i$, $\lambda = 2.3511\varepsilon i$, $\lambda = \mathcal{O}(\varepsilon^2)$ and $\lambda = 0$.

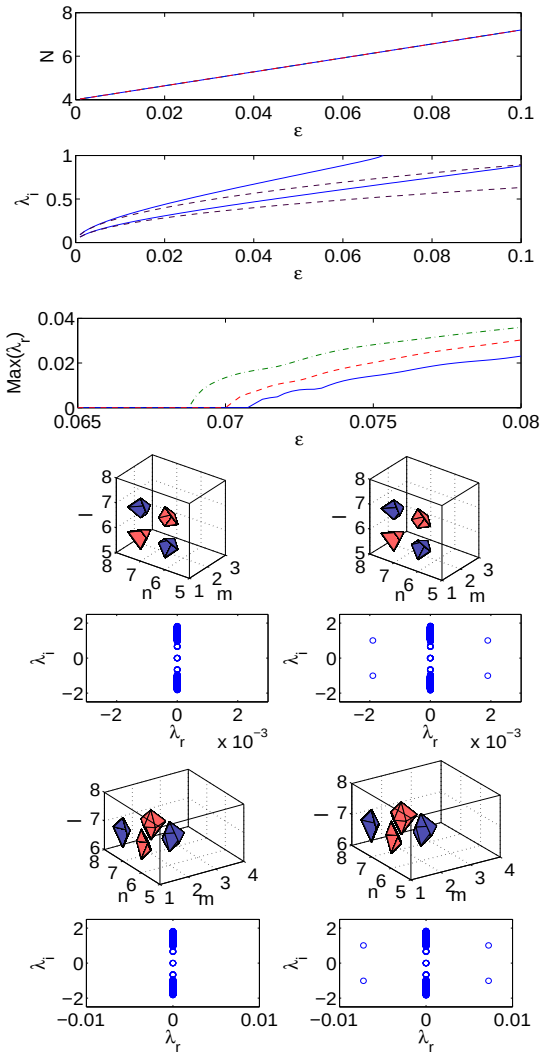

FIG. 4: Stability for the quadrupole. The layout is similar to the one in Fig. 3. In the third panel, due to the close proximity of the thresholds, the panel shows a close-up of the critical stability eigenvalue versus the lattice coupling for the parallel surface mode (solid line), the normal surface mode (dashed line) and the bulk mode (dash-dotted line). The thresholds for the bulk is $\varepsilon = 0.068$, while for the normal and parallel quadrupoles it is, respectively, $\varepsilon = 0.070(1)$ and $\varepsilon = 0.071(1)$. As before, the two set of four panels show the configurations before and after stability along with their corresponding spectral planes.

Next we consider the quadrupole configuration (results depicted in Fig. 4). The surface has again a stabilizing effect, albeit a small one, when the quadrupole is placed normal and parallel to the surface. In the bulk, the quadrupole loses stability at $\varepsilon = 0.068(1)$, while, the normal and parallel surface quadrupoles have stability thresholds located, respectively, at $\varepsilon = 0.070(1)$ and $\varepsilon = 0.071(1)$. The stability eigenvalues can again be computed in this case and are $\lambda = \sqrt{8\varepsilon}i$ (a double eigenvalue) $\lambda = 2\sqrt{\varepsilon}i$, and a zero eigenvalue.

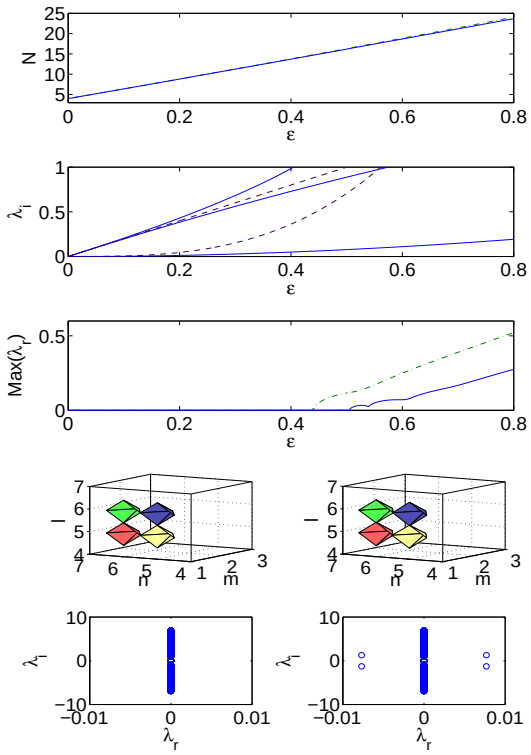

FIG. 5: Stability for the four site vortex in a grid of size $11 \times 11 \times 11$. The dash-dotted line represents the bulk vortex, while the solid line represent the parallel surface version. The layout is similar to those before, with the third the panel being a close-up of the second panel showing a small island of instability for the parallel surface vortex. Instability in the bulk occurs at $\varepsilon = 0.438(1)$, while for the parallel surface vortex the instability occurs at $\varepsilon = 0.505(1)$. Note that a vortex cannot exist normal to the surface. The bottom four panels show the parallel surface vortex before (left, $\varepsilon = 0.485$) and after (right, $\varepsilon = 0.490$) the instability threshold. As in the previous figures, the level contours corresponding to $\mathrm{Re}(u_{l,m,n}) = \pm 0.5 \max\{u_{m,n,l}\}$ are shown, respectively, in blue and red (dark gray and gray, in the black-and-white version), while the imaginary ones, $\mathrm{Im}(u_{l,m,n}) = \pm 0.5 \max\{u_{m,n,l}\}$, are shown by green and yellow (light and very light gray, in the black-and-white version) hues, respectively

In Fig. 5 we present the results for the four site vortex. This configuration, in contrast to the previous ones, is a complex solution. In the AC limit, the vortex occupies the same excited sites as the above mentioned quadrupole but the phase profile emulates a a vortex of charge one with the distribution $\{0, \pi/2, \pi, 3\pi/2\}$ [11, 30]. The bulk four site vortex (which was discussed in [33]) destabilizes at $\varepsilon = 0.438(1)$ while the parallel surface vortex is stabilized further with the threshold of stability at $\varepsilon = 0.505(1)$. The presence of the surface in this case however inhibits the existence of a normal vortex at the surface layer, similarly to what was the case in the 2D counterpart of that structure in [13]. The fact that the surface appears to "push" the vortex away is an interesting feature that it would be particularly valuable (although, it may be equally difficult) to understand theoretically.

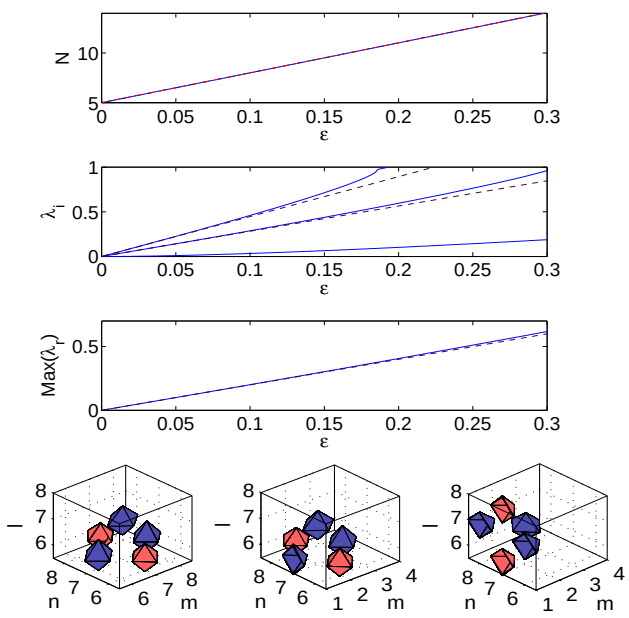

FIG. 6: Stability for the four site pyramid. This configuration consists of a base in the form of a rhombus and an "out of plane" site with zero phase. Three variants of this configuration are displayed in the bottom row of panels (from left to right: bulk, normal and parallel surface). As it can be noticed from the third panel, the stability properties for the three different variants of this pyramid are almost identical. It seen that all three are unstable and that their (in)stability properties are almost identical. The surface is unable to stabilize this type of pyramidal structure, as the instability arises at the lowest order in the eigenvalue calculation.

Finally, we examine a pyramidal structure with characteristics displayed in Fig. 6, which has a base of four sites in a "rhombic" shape. The out of plane site must have phase 0 or π, since the $\pi/2$ and $3\pi/2$ variants do not exist. This set of pyramids (bulk, normal, parallel), are all completely unstable, as seen in the third panel of Fig. 6. The surface has no stabilizing effect in this case (the instability arises at the lowest order in the eigenvalue calculations). Theory yields, eigenvalues $\lambda = 2\sqrt{5}\varepsilon i$, $\lambda = 2\sqrt{2}\varepsilon i$, $\lambda = 2\varepsilon$, $\lambda = 0$ and $\lambda = \mathcal{O}(\varepsilon^2)$.

IV. DYNAMICS

In this section we examine the evolution of the various configurations (see Figs. 7–11). In each case the dynamics is initiated for a value of the coupling ε just beyond the threshold of stability and a perturbation is applied to the initial conditions in order to expedite the onset of the instability.

In each case, we display the evolution of the instability at six different times starting at $t = 0$, and ending

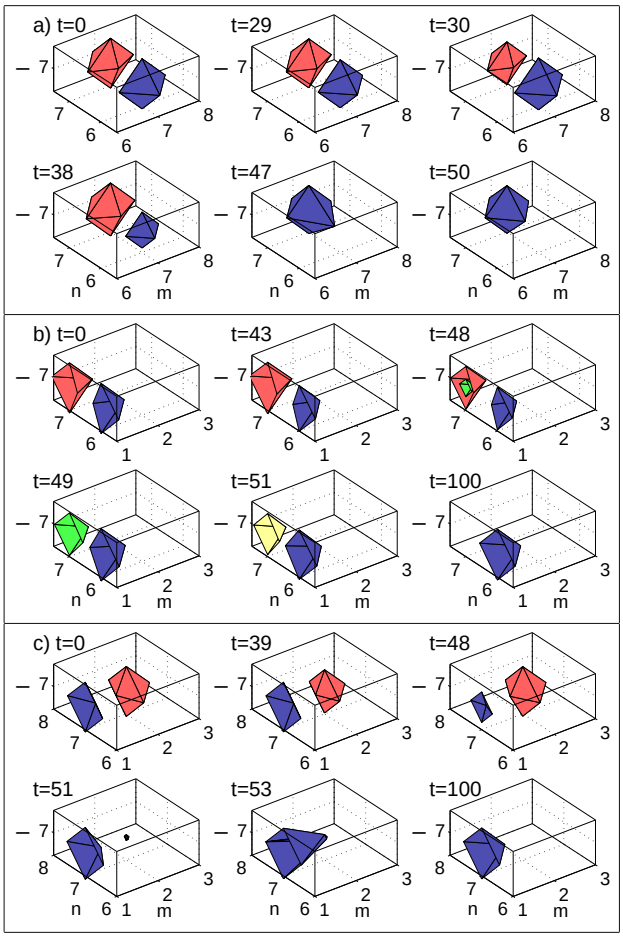

FIG. 7: Dynamics for the unstable dipoles: a) bulk dipole, b) parallel dipole, and c) normal dipole. In all cases the unstable dipole suffers from oscillatory instability that is responsible for the eventual concentration of most of the norm at a single site (i.e., a monopole). The parameters are $\Lambda = 1$, $\varepsilon = 0.2$, the lattice has a size of $13\times13\times13$ and the times are indicated in the panels. All iso-contour plots are done at $\mathrm{Re}(u_{m,n,l}) = \pm0.75 = \mathrm{Im}(u_{m,n,l})$ and the initial steady state configuration was perturbed with a random noise of amplitude 0.01. The color coding for the iso-contours is as follows: blue and red (dark gray and gray, in the black-and-white version) are real iso-contours while the green and yellow (light and very light gray, in the black-and-white version) correspond to imaginary iso-contours.

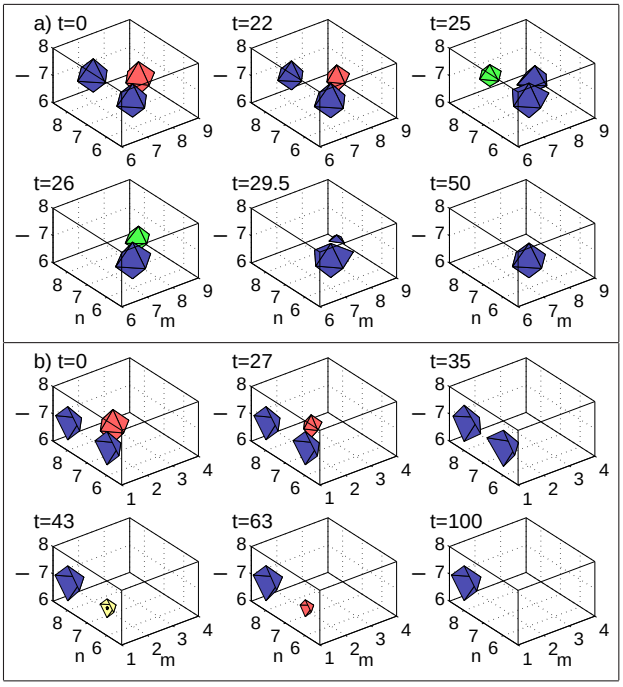

FIG. 8: Dynamics for the unstable 3 site horseshoes: a) bulk 3 site horseshoe and b) normal 3 site horseshoe. For both cases the unstable horseshoe suffers from oscillatory instability that is responsible for the eventual concentration of most of the norm at a single site (i.e., a monopole). The iso-contours and parameters are the same as in Fig. 7 except for $\varepsilon = 0.3$.

at a time well beyond the point at which the instability has manifested itself. All unstable configurations, as predicted by the presence of imaginary parts in the (in)stability eigenvalue λ, exhibit instability dynamics eventually resulting in a different configuration. In the case of the dipoles and horseshoes (see Figs. 7–9), a single site persists, while in the case of the vortex and the pyramid (see Figs. 10–11), a few sites may remain. The single site structure is the most robust dynamical state of the lattice system with the widest interval of stability among the discrete structures; it only becomes unstable (for a given Λ) at the coupling value of $\varepsilon \approx \Lambda$ [33]. Another structure with a relatively wide stability region is the dipole (which is more stable, the wider the distance between its constituent sites), which is consonant with the observation that some of the structures (especially ones with a large number of excited sites, such as vortices and pyramids) dynamically transform into such a waveform. It is important to stress that the exact details of the evolution and *the final state* depend, in general, on the details of the initial perturbation. Each configuration is shown using iso-level contours of different hues. The blue and red (dark gray and gray, in the black-and-white version) are real iso-contours while the green and yellow (light and very light gray, in the black-and-white version) correspond to imaginary iso-contours.

V. CONCLUSIONS

In this work, we have presented a generalization of surface modes in the vicinity of a two-dimensional surface within a three-dimensional prototypical dynamical lattice. We have illustrated that the surface has a variety of interesting properties including the stabilization of structures that are unstable in the bulk (such as 3-site horseshoes), the inhibition of formation of structures that do exist in the bulk (such as vortices normal to the surface, although ones parallel to the surface do exist), and, per-

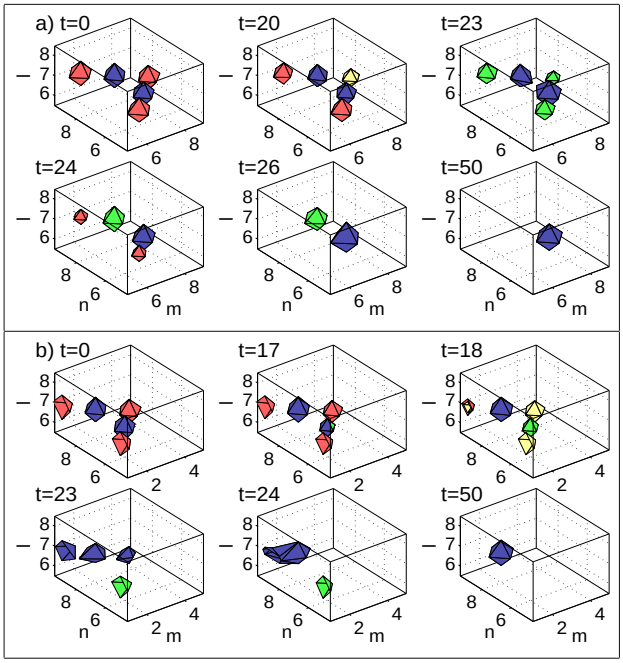

FIG. 9: Dynamics for the unstable 5 site horseshoes: a) bulk 5 site horseshoe and b) normal 5 site horseshoe. For both cases the unstable horseshoe suffers from oscillatory instability that is responsible for the eventual concentration of most of the norm at a single site (i.e., a monopole). The iso-contours and parameters are the same as in Fig. 8.

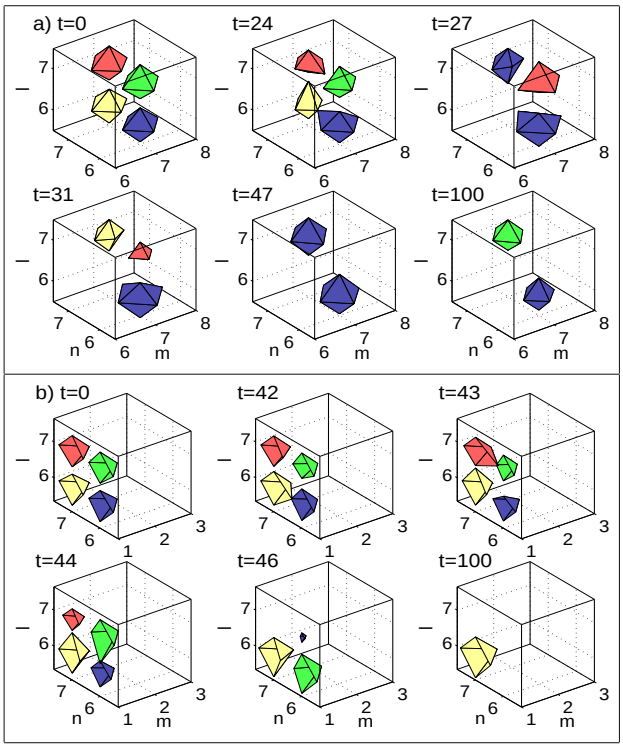

FIG. 10: Dynamics for the unstable vortices: a) bulk vortex for $\varepsilon = 0.3$ and b) parallel surface vortex for $\varepsilon = 0.6$, $\Lambda = 1$ and all iso-contour plots are done at $\mathrm{Re}(u_{m,n,l}) = \pm 1 = \mathrm{Im}(u_{m,n,l})$.

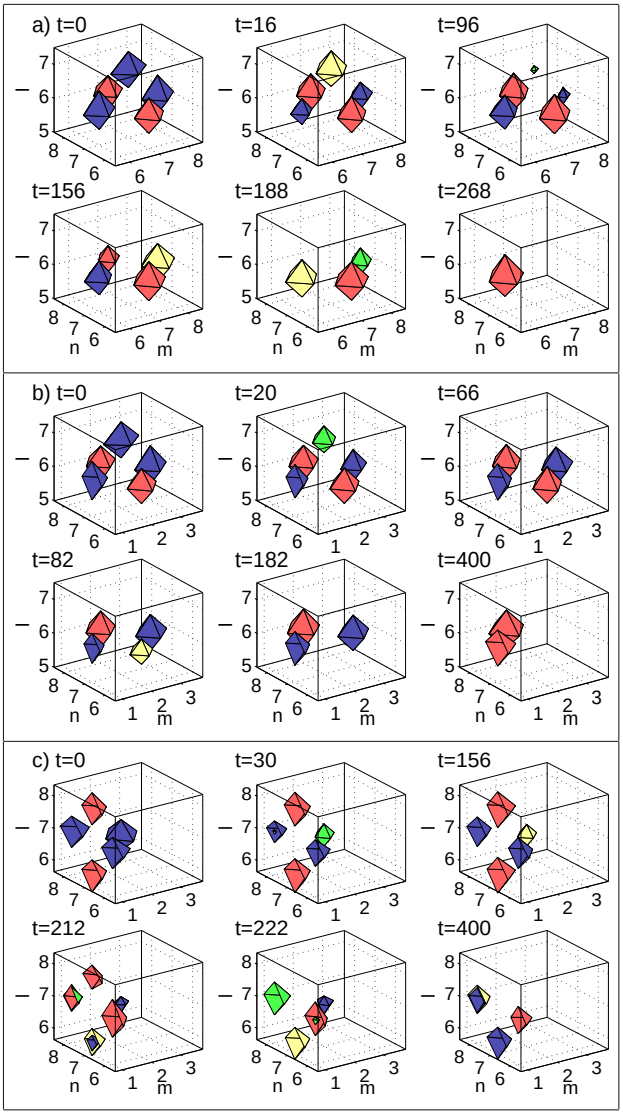

FIG. 11: Dynamics for the unstable pyramids: a) bulk pyramid, b) normal pyramid, and c) parallel pyramid for $\varepsilon = 0.2$.

haps the most typical of its attributes, the expansion of the stability intervals of various solutions that exist in the bulk and survive in the presence of the surface. The latter feature we have attributed to the corresponding decrease (in the presence of the surface) of the number of neighbors that the excited sites encounter, since the approach to the continuum limit is what leads to the instability (or disappearance) of all the stationary structures of this model which possesses no known stable stationary waveforms in its continuum limit.

On the other hand, while the techniques of [30, 32, 34] are quite useful in understanding the dominant stability properties of the solutions, the surface appears to have some particularly subtle effects (such as the stabilization of higher order solutions or the inhibition of some types of vortex structures) which cannot be directly inferred by the bulk considerations of the above works. It would thus

be of particular interest to develop a version of the existence and stability techniques based on the Lyapunov-Schmidt reductions of [30, 32, 34] which accounts for the effects of the surface. Such a development may shed light on the nature of configurations that may be inhibited or stabilized by the surface.

[1] W.L. Barnes, A. Dereux and T.W. Ebbesen, Nature **424**, 824-830 (2003).

[2] D.N. Christodoulides, F. Lederer and Y. Silberberg, Nature **424**, 817-823 (2003).

[3] S. Bohlius, H.R. Brand and H. Pleiner, Z. Phys Chem. **220**, 97-104 (2006).

[4] K.G. Makris, S. Suntsov and D.N. Christodoulides, G.I. Stegeman, Opt. Lett. **30**, 2466 (2005); M.I. Molina, R.A. Vicencio, and Y.S. Kivshar, Opt. Lett. **31**, 1693 (2006).

[5] S. Suntsov, K.G. Makris, D.N. Christodoulides, G.I. Stegeman, A. Hache, R. Morandotti, H. Yang, G. Salamo, and M. Sorel, Phys. Rev. Lett. **96**, 063901 (2006).

[6] Y.V. Kartashov, V.A. Vysloukh and L. Torner, Phys. Rev. Lett. **96**, 073901 (2006).

[7] G. Sivilogou, K.G. Makris, R. Iwanow, R. Schiek, D.N. Christodoulides, G.I. Stegeman, Y. Min, and W. Sohler, Opt. Exp. **14**, 5508 (2006).

[8] C.R. Rosberg, D.N. Neshev, W. Krolikowski, A. Mitchell, R.A. Vicencio, M.I. Molina, and Yu.S. Kivshar, Phys. Rev. Lett. **97**, 083901 (2006)

[9] E. Smirnov, M. Stepic, C.E. Rüter, D. Kip, V. Shandarov, Opt. Lett. **31**, 2338 (2006).

[10] Y.V. Kartashov, A.A. Egorov, V.A. Vysloukh, and L. Torner, Opt. Exp. **14**, 4049 (2006).

[11] B.A. Malomed, and P.G. Kevrekidis, Phys. Rev. E. **64**, 026601 (2001).

[12] D.N. Neshev, T.J. Alexander, E.A. Ostrovskaya, Y.S. Kivshar H. Martin, I. Makasyuk, and Z. Chen Opt. Phys. Rev. Lett. 92, 123903 (2004).

[13] H. Susanto, and P.G. Keverekidis, B.A. Malomed, R. Carretero-Gonzalez, and D.J. Frantzeskakis, Phys. Rev. E. **72**, 046613 (2005).

[14] K.G. Makris, J. Hudock, D.N. Christodoulides, G.I. Stegeman, O. Manela and M. Segev, Opt. Lett. **31**, 2274 (2006).

[15] Y.V. Kartashov and L. Torner, Opt. Lett. **31**, 2172 (2006).

[16] R.A. Vicencio, S. Flach, M.I. Molina and Yu.S. Kivshar, Phys. Lett. A **364**, 274 (2007).

[17] X. Wang, A. Bezryadina, Z. Chen, K.G. Makris, D.N. Christodoulides and G. Stegeman, Phys. Rev. Lett. **98**, 123903 (2007).

[18] A. Szameit, Y.V. Kartashov, F. Dreisow, T. Pertsch, S. Nolte, A. Tünnermann and L. Torner, Phys. Rev. Lett. **98**, 173903 (2007).

[19] Y.V. Kartashov, V.A. Vysloukh and L. Torner, Phys. Rev. A **76**, 013831 (2007).

[20] Mario I. Molina, Yaroslav V. Kartashov, Lluis Torner, Yuri S. Kivshar, arXiv:0712.3179.

[21] A. Namdar, I.V. Shadrivov and Yu.S. Kivshar, Phys. Rev. A **75**, 053812 (2007).

[22] B. Alfassi, C. Rotschild, O. Manela, M. Segev, and D.N. Christodoulides, Phys. Rev. Lett. **98**, 213901 (2007).

[23] F. Ye, Y.V. Kartashov and Lluis Torner, arXiv:0802.2521.

[24] D. Mihalache, D. Mazilu, F. Lederer and Yu.S. Kivshar, Opt. Lett. **32**, 3173 (2007).

[25] D. Mihalache, D. Mazilu, F. Lederer and Yu.S. Kivshar, Opt. Lett. **32**, 2091 (2007).

[26] J.E. Heebner and R.W. Boyd, J. Mod. Opt. **49**, 2629 (2002); P. Chak, J.E. Sipe and S. Pereira, Opt. Lett. **28**, 1966 (2003).

[27] J.J. Baumberg, P.G. Savvidis, R.M. Stevenson, A.I. Tartakovskii, M.S. Skolnick, D.M. Whittaker and J.S. Roberts, Phys. Rev. B **62**, R16247 (2000); P.G. Savvidis and P.G. Lagoudakis, Semicond. Sci. Technol. **18**, S311 (2003).

[28] O. Morsch and M. Oberthaler, Rev. Mod. Phys. **78**, 179 (2006).

[29] I. Bloch, Nature Phys. **1**, 23 (2005).

[30] D.E. Pelinovsky, and P.G. Kevrekidis, and D.J. Frantzeskakis, Physica D **212**, 20 (2005).

[31] M. Golubitsky, and D.G. Schaeffer, and I. Stewert, Singularities and Groups in Bifurcation Theory, vol.1, Springer Verlag, New York, 1985.

[32] D.E. Pelinovsky, and P.G. Kevrekidis, and D.J. Frantzeskakis, Physica D **212**, 1 (2005).

[33] P.G. Kevrekidis, B.A. Malomed, D.J. Frantzeskakis and R. Carretero-González, Phys. Rev. Lett. **93**, 080403 (2004).

[34] M. Lukas, D. Pelinovsky and P.G. Kevrekidis, Physica D **237**, 339 (2008).